



Design and analysis of a multi-band miniaturized metamaterial absorber for wireless communication applications

Karim Errajaji¹ · Nawfal Jebbor¹ · Sudipta Das² · Tanvir Islam³ · Boddapati Taraka Phani Madhav⁴ · Tarik El-Arrouch⁵

Received: 13 October 2023 / Accepted: 13 November 2023 / Published online: 26 December 2023
© The Author(s), under exclusive licence to Springer Science+Business Media, LLC, part of Springer Nature 2023

Abstract

This article presents a compact metamaterial absorber that operates at hepta-bands within the microwave frequency spectrum exhibiting more than 85% absorption at each band. The design of this absorber is based on the combination of three resonators that offer seven peaks at 3.15, 5.96, 8.73, 9.36, 13.22, 13.71, and 14.45 GHz with an absorption of 93.65, 85.75, 94.14, 99.51, 90.55, 97.87, and 98.68%, respectively. This absorber is characterized by a unit cell of size $0.168\lambda_0 \times 0.168\lambda_0$ and a thickness of $\lambda_0/59.5$ calculated at 3.15 GHz. The overlap between the absorption bands provided by each resonator gives rise to a wide full wave at half maximum bandwidths of 0.20, 0.19, 0.64, and 2.04 GHz within microwave S, C, X, Ku-bands respectively. All three resonators utilized in designing the structure are symmetrical, which makes this structure insensitive to polarization for both transverse electric and transverse magnetic modes. To understand the origin of each absorption band, characteristic impedance, surface current, and distribution of the electromagnetic field are analyzed for all the absorption bands. Further, an electrical equivalent model (ECM) diagram is obtained by implying the ADS tool and the results of ECM analysis are compared with the results obtained by HFSS simulator. Finally, the prototype of the suggested design is fabricated and the measured results are compared with the theoretical results, which validates the design approach of this specific metamaterial (MTM)-based absorber model. The prescribed MTM absorber features effective characteristics for sensing and various wireless communication applications in microwave frequency regions.

Keywords Absorber · FWHM · Hepta-band · Metamaterial · Microwave bands · Polarization · Wireless communication

1 Introduction

During World War II, scientific research focused on designing electromagnetic (EM) wave absorbers to minimize the signature of air craft and submarines' periscopes. Since the first conception of absorbers, researchers are working rigorously to provide significant solutions for designing high quality absorbers to meet the advanced requirements of modern

wireless communication applications. As an effective solution, with the advent of metamaterials, remarkable changes have been witnessed in design principle and electromagnetic characteristics of the absorbers. The metamaterial absorbers (MMAs) offer several advantages such as reduced mass and low thickness and can be made from standard materials widely used in the industry unlike the conventional absorbers such as magnetic absorbers (Michielssen et al. 1993), analog circuit-based absorbers (Gau et al. 1997), and structural absorbers (Zadeh and Karlsson 2009). In modern times, MMAs find applications in various fields such as Communication (Hannan et al. 2022b), Biomedical (Abdulkarim et al. 2022), Sensing (EL-Wasif et al. 2023), Solar energy (Wu et al. 2022), and shielding (Zhang et al. 2020).

Generally, when an MMA structure is exposed to an EM wave, it exhibits negative permeability or negative permittivity, or both (Hrabar 2006; Ziolkowski 2003). Therefore, it absorbs the maximum of EM waves if there is proper matching between its characteristic impedance and the impedance of the free space, hence a low coefficient of transmission and reflection. Three layers typically make up an MMA structure: a metallic material forms the top (patch) and bottom (ground plane) layers, with a dielectric substrate situated in the between. Regarding the choice of substrate, various studies have utilized commercial substrates such as Rogers RO or RT and FR-4 (Hannan et al. 2020). Additionally, MMAs can be designed using double and multi-layers (Saadeldin et al. 2023; Ren et al. 2020; Zhang et al. 2020). These materials find applications across different frequency ranges, including optics, infrared, terahertz, and microwave (Mahmud et al. 2020; Shuvo et al. 2022; Lv et al. 2022; Abouelez and Abdulaleem 2023).

In the microwave field, MMAs can be used in many applications, including absorption of radar waves, improvement of antenna performance, or reduction of electromagnetic interference (Moniruzzaman et al. 2020; Hakim et al. 2023; Ali et al. 2022b; Munaga et al. 2015). In Landy et al. (2009). For the first time, a double-negative MMA with an absorbance of 88% is reported that operates in the microwave range and specifically in the X application band, this MMA used a split ring resonator (SRR) as a base. After that, scientific researches have been expanded which brings different varieties of MMAs that work in several bands of applications like, S, C, X, and Ku (Hakim et al. 2022). The recommended MMA for Ku band application is based on a modified square SRR. The dimension of this absorber unit cell is $0.44\lambda \times 0.44\lambda \times 0.088\lambda$, where λ is the wave length at the lower resonance frequency, it can reach two absorption peaks of 99.99% in the Ku-band with an average bandwidth absorption of 420 MHz and 480 MHz, respectively. In Hossain et al. (2022), a double E-shaped symmetric SRR MMA is proposed. The electrical size of this unit cell is $0.179\lambda \times 0.179\lambda$ and it is able to absorb in all three regions in the S and C-bands with an average absorption greater than 99%. Moreover, this structure shows an almost perfect absorption profile across a broad angle of incidence up to 60° in both modes (TM and TE). A double elliptical resonator is proposed in Hossain et al. (2023). The quad-band absorption achieved a wide range of polarization angle up to 60° for TE mode. A penta band MMA is presented in Hannan et al. (2021) which is made of a swastika-shaped patch with a size of $0.169\lambda \times 0.169\lambda$, and can absorb EM waves belonging to the bands X, C, and Ku. Further, this absorber presents an absorption spectrum that does not depend on the co-polarized and cross-polarized EM waves, and the refractive indices are near zero at resonance frequencies. An MMA is presented in Ali et al. (2022a) which is based on the combination of three Closed Circular Ring Resonators (CCRR). The size of this absorber is $22\text{ mm} \times 22\text{ mm}$ and it shows polarization-independent characteristics for TE and TM modes. This absorber provides six resonance frequencies for C and X application bands. The MMA presented in Dewangan and Mishra (2023) requires a total dimension of $0.32\lambda \times 0.32\lambda \times 0.098\lambda$ based on a combination of L-shaped resonators.

This structure provides three peaks of absorption in X, Ku-bands. The absorption profile is shown over a wide polarization angle and incidence up to 50° for TE and 60° for TM modes. This brief review of the scientific literature reveals that the current focus is on developing multiband MMAs with desirable properties like a broad bandwidth FWHM, high absorption, high stability depending on the polarization state of the EM wave and the angle of incidence. But achieving all these characteristics for a monolayer absorber based on an FR4 substrate remains a challenge.

In this article, a compact MMA using the classical low cost FR4 substrate is presented. This structure is based on the capacitive coupling between three resonators that offers seven peaks of absorption in the microwave S, C, X, and Ku-bands. The unit cell of this MMA achieves insensitive polarization, and a wide angle of incidence for both TE and TM modes which reaches up to 50° . Various characteristics parameters such as permittivity of dielectric and magnetic permeability are extracted and analyzed in order to verify the metamaterial behavior of this absorber. The analysis of the field (E and H) and surface current distributions are carried out and discussed to offer an intuitive discussion of the absorption mechanism. Furthermore, numerous parametric analyses are executed to study the geometric effect of the patch on the absorption spectrum. The proposed MMA offers several advantages as outlined follows:

- The MMA provides seven absorption bands, characterized by broad polarization independence.
- A wide total bandwidth FWHM of 3.07 GHz in S, C, X, Ku-bands.
- The absorber requires a compact electrical size of $0.168\lambda_0 \times 0.168\lambda_0$.
- The proposed absorber exhibits more than 85% absorption for all operating the bands.
- The prescribed absorber is suitable for sensing and wireless communication applications operating within microwave S, C, X, Ku-bands.

2 Design and evolution of MMA cell

The unit cell for the MMA proposed in this work is shown with different views as depicted in Fig. 1. Copper as conducting material and the FR4 as the dielectric materials are employed in the fabrication of the absorber. Copper with an electrical conductivity of $\sigma = 5.8 \times 10^7 \text{ Sm}^{-1}$ and thickness of $t = 0.035 \text{ mm}$ is used to make the patch and the ground layer. The FR4 with a tangent loss of 0.02, a dielectric constant of $\epsilon_r = 4.4$, and a thickness $h = 1.6 \text{ mm}$ is placed in the middle of the configured structure. The patch is produced by a combination of three resonators: a twisted square ring (Resonator-A), a modified cross (Resonator-B), and L-shaped chopsticks (Resonator-C). The parameters optimized for this MMA cell to achieve maximum absorption are detailed in Table 1.

The Ansys-HFSS-2022 software is used to design the suggested MMA unit cell under periodic boundaries. As shown in Fig. 2, primary and secondary boundary conditions have been applied in the x and y directions, while excitation is applied using the Floquet Port along the z-direction.

The absorption coefficient can be calculated at different frequencies by mathematical Eq. (1):

$$A(f) = R(f) - T(f) \quad (1)$$

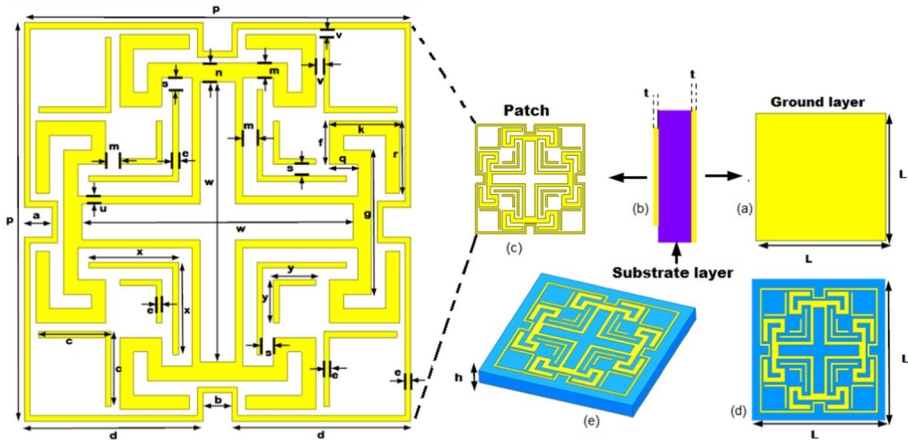
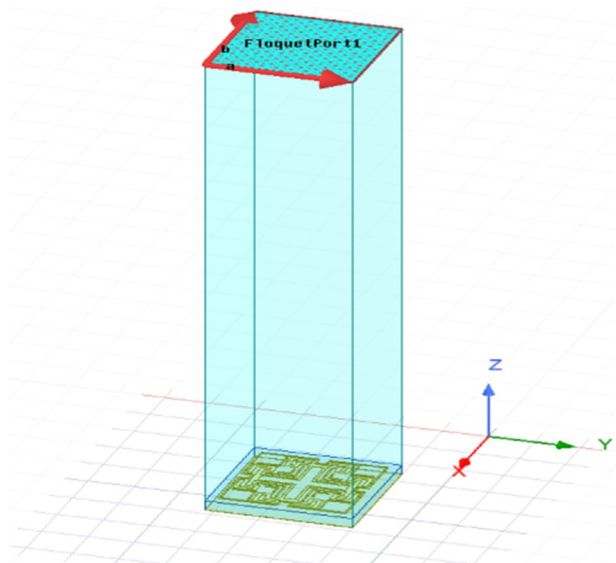


Fig. 1 Multiple perspectives of the suggested unit cell **a** bottom side, **b** side side, **c** various parameters of the patch, **d** upper view, **e** isometric view

Table 1 Dimensions in (mm) required for unit cell patch

Parameter	Value	Parameter	Value	Parameter	Value	Parameter	Value
L	16	c	2.6	k	2.5	y	1.5
p	13.8	d	6.45	n	0.75	s	0.45
w	9.5	e	0.2	m	0.45	q	1
a	1.06	f	1.5	u	0.32	v	0.3
b	0.9	g	5	x	3.2		

Fig. 2 Configuration of the unit cell simulated in HFSS



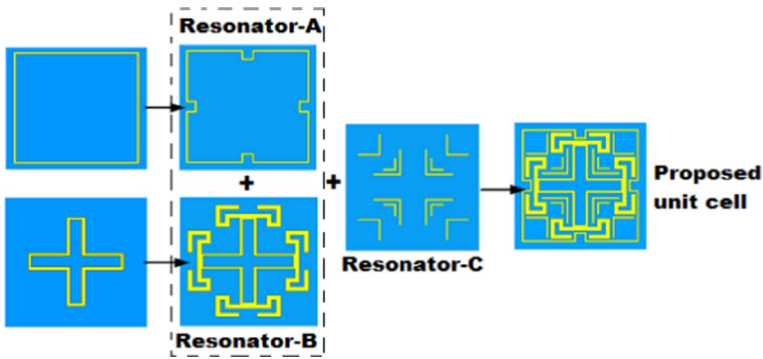


Fig. 3 Development stages of the prescribed unit cell design

where $R(f) = |S_{11}|^2$ and $T(f) = |S_{21}|^2$ are the coefficients of reflection and transmission, respectively. Since the background of this MMA structure is made of copper of thickness $t = 0.035$ mm which is much larger than the skin depth, this allows to neglect the transmission of the EM wave through this structure, hence, the Eq. (1) is reduced as follows:

$$A(f) = 1 - R(f) \tag{2}$$

So, the coefficient of absorption is near to unity ($A = 1$) if the coefficient of reflection equals zero ($R = 0$).

Figure 3 illustrates the design progression steps of the unit cell, while Fig. 4 provides the absorption profile for each resonator. It is remarkable that Resonator-A exhibits three distinct absorption peaks within the S, X, and Ku frequency bands, achieving absorption rates of 98.83, 74.75, and 99.69% at frequencies of 2.80, 9.21, and 13.86 GHz, respectively. Resonator-B contributes to absorption in four frequency bands: S, C, X, and Ku, with absorption percentages of 96.83, 95.77, 98.25, and 84.80% at 2.98, 6.41, 9.59, and 14.18 GHz, respectively. Furthermore, Resonator-C gives dual-band absorption in the Ku-band at 12.71 and 14.04 GHz, with absorption rates of 72.72 and 99.96%, respectively. The two Resonators-B and -C are therefore placed inside the Resonator-A to produce the suggested MMA unit cell whose absorption characteristics are shown in Fig. 5. It appears that

Fig. 4 The absorption profile for Resonator-A, Resonator-B, Resonator-C

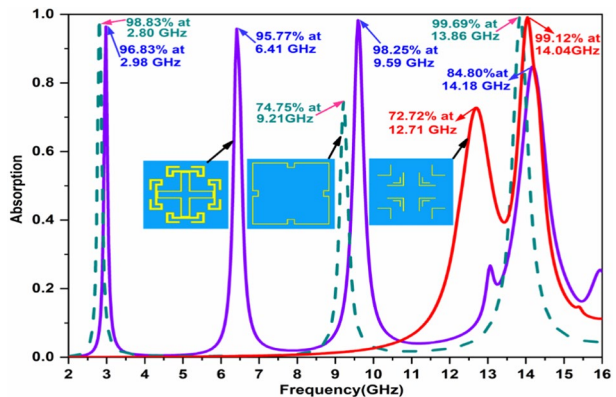
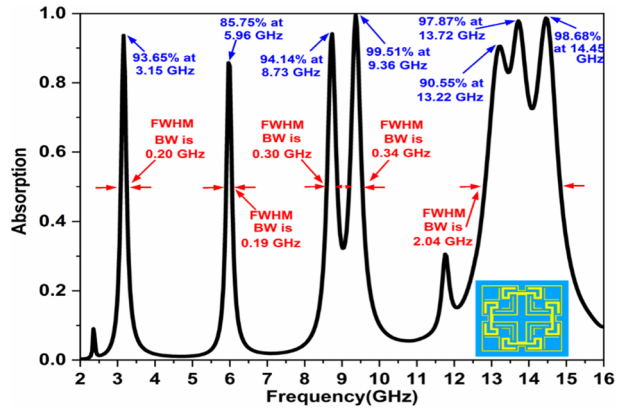


Fig. 5 The absorption profile for the proposed unit cell



absorber offers a total of seven absorption peaks distributed across in the S, C, X, and Ku frequency bands. Because of the capacitive coupling between these three resonators, the absorption peaks are displaced, diminished, increased, and disappeared. In S-band the coupling between two Resonators A and B gives rise to an absorption peak at 3.15 GHz with 93.65% and a low peak of 9% at 2.35 GHz. The absorption peak of 85.75% at 5.96 GHz is provided by Resonator-B alone in the C-band, while the two Resonators A and B offer two absorption peaks of 94.14 and 99.51% at 8.73 GHz and 9.36 GHz, respectively in the X-band. Therefore, the three Resonators A, B, and C is responsible for the appearance of three peaks in the Ku-band at 13.22, 13.71, and 14.45 GHz with an absorbance of 90.55, 97.87, and 98.68%. Moreover, a low peak has appeared at 11.98 GHz with an absorbance of 30%. A major advantage of this suggested MMA structure is a large width at half maximum (FWHM), especially in the Ku-band, which is close to 2.04 GHz. Table 2 shows the detailed FWHM at each absorption band for this proposed absorber.

3 Verification of the metamaterial behavior of this absorber

Equation (3) describes the mathematical relationship between the reflection coefficient $r(f)$ and the input impedance of the MMA structure $Z_a(f)$ which depends on the geometry of the patch, and the impedance of the free space Z_0 :

Table 2 Simulated result of the suggested unit cell

Bands	Resonance frequency (GHz)	Absorption (%)	FWHM bandwidth (GHz)
S	3.15	93.65	0.20 (3.18–2.98 GHz)
C	5.96	85.75	0.19 (5.88–6.07 GHz)
X	8.73	94.14	0.30 (8.57–8.87 GHz)
	9.36	99.51	0.34 (9.53–9.19 GHz)
	13.22	90.55	
Ku	13.71	97.87	2.04 (14.84–12.80 GHz)
	14.45	98.68	

$$r(f) = \frac{Z_a(f) - Z_0}{Z_a(f) + Z_0} \tag{3}$$

where the input impedance can be expressed by the following relationship:

$$Z_a(f) = Z_0 \sqrt{\frac{\mu_r(f)}{\epsilon_r(f)}} \tag{4}$$

$$Z_0 = \sqrt{\frac{\mu_0}{\epsilon_0}} = 377 \Omega \tag{5}$$

where $\mu_r(f)$ is the relative permittivity as a function of frequency, μ_0 and ϵ_0 are two physical constants, respectively the permeability and permittivity of the vacuum. It is already mentioned, the absorber is perfect if the reflection coefficient equals to zero. Figure 6a depicts the variations in normalized input impedance for the 2–16 GHz frequency range. Additionally, for each resonant frequency, Table 3 summarizes the values of the imaginary and real parts of the normalized input impedance. It indicates strong absorption at these frequencies by showcasing close to unity real parts and close to zero imaginary parts.

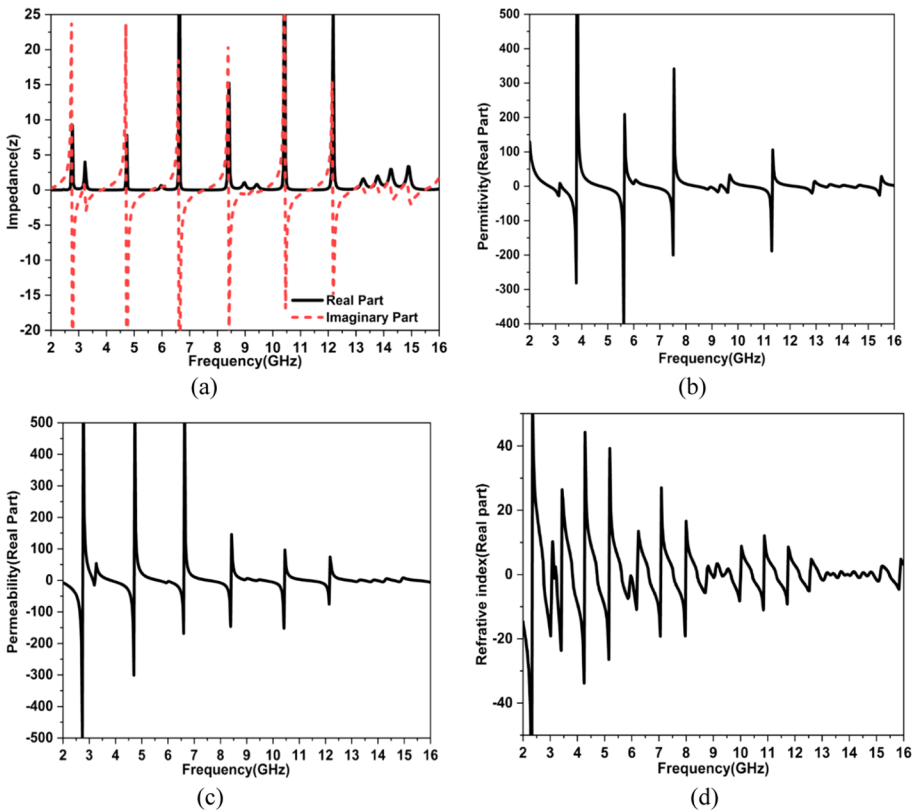


Fig. 6 **a** Normalized impedance, **b** relative permittivity, **c** relative permeability, **d** refractive index for the unit cell

Table 3 Values of permittivity, permeability, refractive index and normalized impedance

Absorption (GHz)	Re (ϵ_r)	Re (μ_r)	n_r	Re (z)	Im (z)
3.15	9.89	-5.32	-1.18	0.67	0.28
5.96	7.76	-5.44	-0.84	0.63	0.54
8.73	-1.68	3.27	-0.39	1.30	-0.47
9.36	-5.15	2.95	0.72	0.87	0.018
13.22	-2.15	2.99	-0.093	1.35	-0.66
13.71	-0.76	1.14	-0.42	1.19	-0.26
14.45	-0.54	0.36	0.044	0.81	-0.087

To verify the metamaterial property of this absorber, permittivity, and permeability are (Nicolson–Ross–Weir) process according to the Eqs. (6–8) (Luukkonen et al. 2011). Due to the ground plane, the transmission of the electromagnetic wave is negligible, so that $S_{21} = 0$. The S_{11} values are therefore taken for the TEM mode at normal incidence. The Permittivity (ϵ_r), permeability (μ_r), and the refractive index (n_r) can be found by using the MATLAB codes developed for the referred relationships. The results indicate that the imaginary parts of the permittivity and permeability are simultaneously negative, which is not consistent with the Lorentz model generally used to study MTMs. These results therefore contradict the fundamental principles of physics. It is possible that these results are due to approximation and truncation and round off errors (Woodley and Mojahedi 2010). So, the imaginary components have not been taken in to account. The real parts of the permittivity, permeability and the relative index is plotted in Fig. 6b–d. For more details. Table 3 shows the values of these physical quantities at each resonance frequency. It is clear that the absorber under consideration exhibits a single negative (SNG) characteristic, the permeability or permeability is negative. In addition, the refractive index for each resonance frequency is close to zero or negative, confirming the metamaterial behavior of this absorber.

$$\epsilon_r = \frac{2}{jk_0h} \frac{1 - (S_{21} + S_{11})}{1 + (S_{21} + S_{11})} \tag{6}$$

$$\mu_r = \frac{2}{jk_0h} \frac{1 - (S_{21} - S_{11})}{1 + (S_{21} - S_{11})} \tag{7}$$

$$n_r = \text{real} \left(\frac{c}{j\pi fh} \sqrt{\frac{(S_{21} - 1)^2 - (S_{11})^2}{(S_{21} - 1)^2 + (S_{11})^2}} \right) \tag{8}$$

4 Performance analysis of designed MMA

This section explores the effects of electromagnetic (EM) wave polarization and oblique incidence on the absorption profile of the suggested MMA. Figure 7 shows the absorption spectrum for two polarization modes, TE and TM, under conditions of normal incidence, with

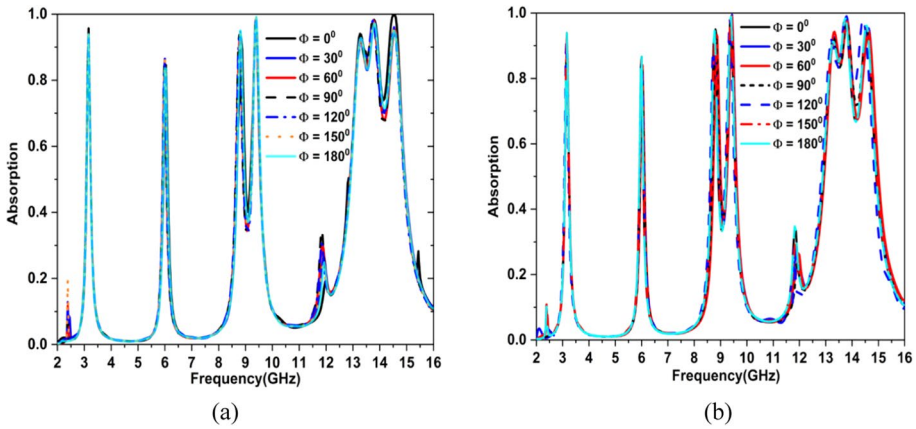


Fig. 7 The impact of polarization angle variations on the absorption spectrum **a** TE mode, **b** TM mode

polarization angles (Φ) ranging from 0° to 180° with an increment of 30° . It is observable that for all values of the polarization angle, the absorption profile behavior is not affected for both modes. This is due to the structural symmetry of the three resonators. Further, the absorption behavior of various oblique incidence angles (Θ) which ranges from 0° to 50° with a step of 10° for both polarization modes TE and TM is also presented in Fig. 8. It can be seen that the first four peaks of absorption of the S, C, and X bands are greater than 70% up to the incidence angle of 50° for both modes. Whereas for the Ku-band, when the angle of incidence exceeds the value 15° , several absorption bands appear. It is also remarkable that the two spurious absorption bands appear for large incidence angles at 6.6 GHz and 10.6 GHz for TE mode. On the other hand, another spurious absorption band at 11.4 GHz increases and shifts towards the lower frequencies for TM mode. This spurious absorption is probably due to the cross-coupling, between the resonators, the electrical excitation for TM polarization, and the magnetic excitation for TE polarization, which may because of the diminution of absorptions for high incidence angles (Chaurasiya et al. 2016). Furthermore, in accordance with Eqs. (9) and (10), the reflection coefficient for TE and TM modes depends on both the angle of incidence (θ_i)

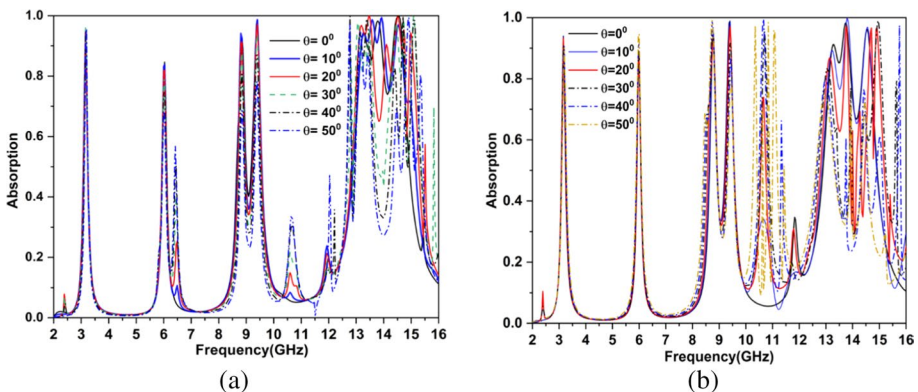


Fig. 8 The impact of angle of incidence variations on the absorption spectrum **a** TE mode, **b** TM mode

and the angle of transmission (θ_t) (Balanis 2012). Clearly, as the θ_i varies, the reflection coefficient fluctuates intrinsically, leading to a decrease in the level of absorption.

$$\Gamma_{TE} = \frac{Z_a \cos \theta_i - Z_0 \cos \theta_t}{Z_a \cos \theta_i + Z_0 \cos \theta_t} \tag{9}$$

$$\Gamma_{TM} = \frac{Z_a \cos \theta_t - Z_0 \cos \theta_i}{Z_a \cos \theta_t + Z_0 \cos \theta_i} \tag{10}$$

One of the criteria for considering an absorber to be perfect is its ability to absorb EM waves for both co-polarized and cross-polarized modes (Kong et al. 2019). Similarly, no EM waves pass through this MMA structure because of the copper ground plane. Moreover, the reflection coefficient depends on two types of EM waves, as shown by the following equation:

$$A(f) = 1 - |S_{11xx}|^2 + |S_{11xy}|^2 \tag{11}$$

where $R_{xx} = |S_{11xx}|^2$ and $R_{xy} = |S_{11xy}|^2$ are the corresponding reflection coefficients for co- and cross-polarized EM waves respectively. The S_{11xx} and S_{11xy} parameters for TEM mode under normal incidence are displayed in Fig. 9a. As the cross-polarized S_{11xy} parameter is of very low values, so the absorption of the designed MMA is affected by the cross-polarized waves as represented in Fig. 9b.

The Ampere and Faraday Maxwell equations (12, 13) as well as the two medium Eqs. (15, 16) may be utilized to explain how the EM wave interaction with the absorbing metamaterial (Paul 2009, Wartak et al. 2011)

$$\nabla \times H = J + \frac{\partial D}{\partial t} \tag{12}$$

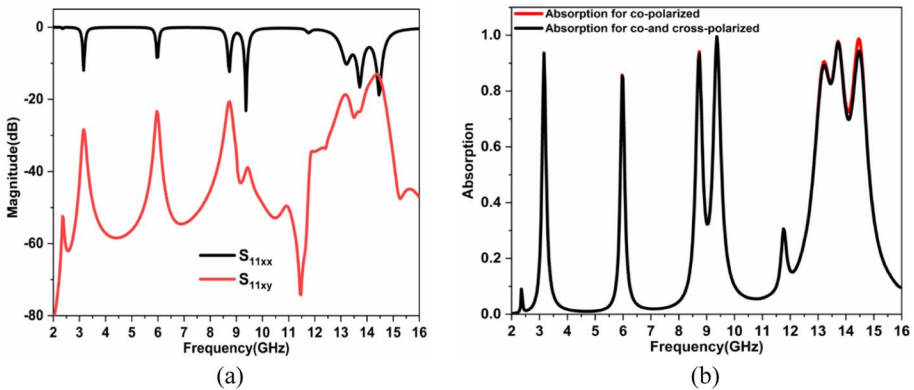


Fig. 9 **a** S_{11xx} and S_{11xy} parameters for TEM mode under normal incidence, **b** absorption for co-polar and both co and cross-polar

$$\nabla \times E = -\frac{\partial B}{\partial t} \quad (13)$$

where

$$\nabla = \left[\frac{\partial}{\partial x}, \frac{\partial}{\partial y}, \frac{\partial}{\partial z} \right] \quad (14)$$

$$D(t) = \varepsilon \cdot E(t) \quad (15)$$

$$B(t) = \mu \cdot H(t) \quad (16)$$

To comprehend the absorption mechanism, it is crucial to analyze the EM field distribution on each part of each resonator. In this section, a detailed discussion is delivered for the results shown in Fig. 10. The electric field is identified on the right and left sides of both Resonators A and B at 3.15 GHz. This corresponds to the fact that the first absorption band is caused by the combined contribution of these two resonators. For 5.96 GHz frequency, the E-field is focused on the highest and lowest sides of Resonator B, so the generation of second absorption band is due to presence of this resonator. At 8.73 GHz, the stronger E-field appears at the top of the left and right square parts of the Resonator-A, and at the top and bottom of the linear parts of the Resonator-B. At 9.36 GHz, the E-field appears to converge towards the center and extends to both the left and right sides of Resonator-B, and further on the two square parts upper left and right of the Resonator-A indicating that the third and fourth absorption peaks within the X-band are due to the contribution of Resonators A and B. In Ku-band, strong E-fields are observed on the various areas of three resonators. This confirms that the three peaks of this band are generated by the coupling of three Resonators A, B, and C. At 13.22 GHz, a significant E-field strength appears on the four internal edges L-shaped resonator and on the middle of corners Resonator-B, and on two square parts at upper left and right of the Resonator-A. On the four inner and outer edges of the L-shaped resonator, the electric field is much centered at 13.71 GHz. Finally, for the last absorption band at 14.45 GHz, the E-field is located on the upper most left and right sides of square part Resonator-A, as well as along both the exterior and interior edges of Resonator-C. According to the Maxwell equations as referred, two electric and magnetic fields are coupled. This means that the variation of the E-field as a function of time creates a curl of the H-field. Figure 10 also shows the distribution of the H-field at each resonance frequency. It can be observed that the H-field is near to zero when the E-field constant, and the presence of the H-field is also noticed when the E-field changes. Furthermore, the comparison of the distributed surface current and the H-field pattern reveals that the intensified H-field is present in the region of the high current density.

Additionally, to investigate the absorption properties of the MMA, the equivalent circuit model (ECM) of the designed MTM unit cell is presented in Fig. 11. Each RLC circuit functions as a resonator for each resonance frequency, the inductance (L) represents the ability of the MMA to store magnetic energy, while the capacitor (C) is used to represent the ability of an MMA to store electrical energy. Resistance (R) simulates energy loss within the absorber. The RLC (R_8, L_8, C_{15}) circuit functions as a resonator for the copper solid masse. Then for the capacitors ($C_{2,4,6,8,10,12,14,16}$), its role is to provide isolation between two adjacent resonances. To obtain the desired S11, all circuit element values are fine-tuned on ADS (Hannan et al. 2022a, c): $L_1 = 109.6$ nH, $L_2 = 12.1$ nH, $L_3 = 14.9$ nH, $L_4 = 16.51$ nH, $L_5 = 7.611$ nH, $L_6 = 10.4181$ nH, $L_7 = 10.7536$ nH,

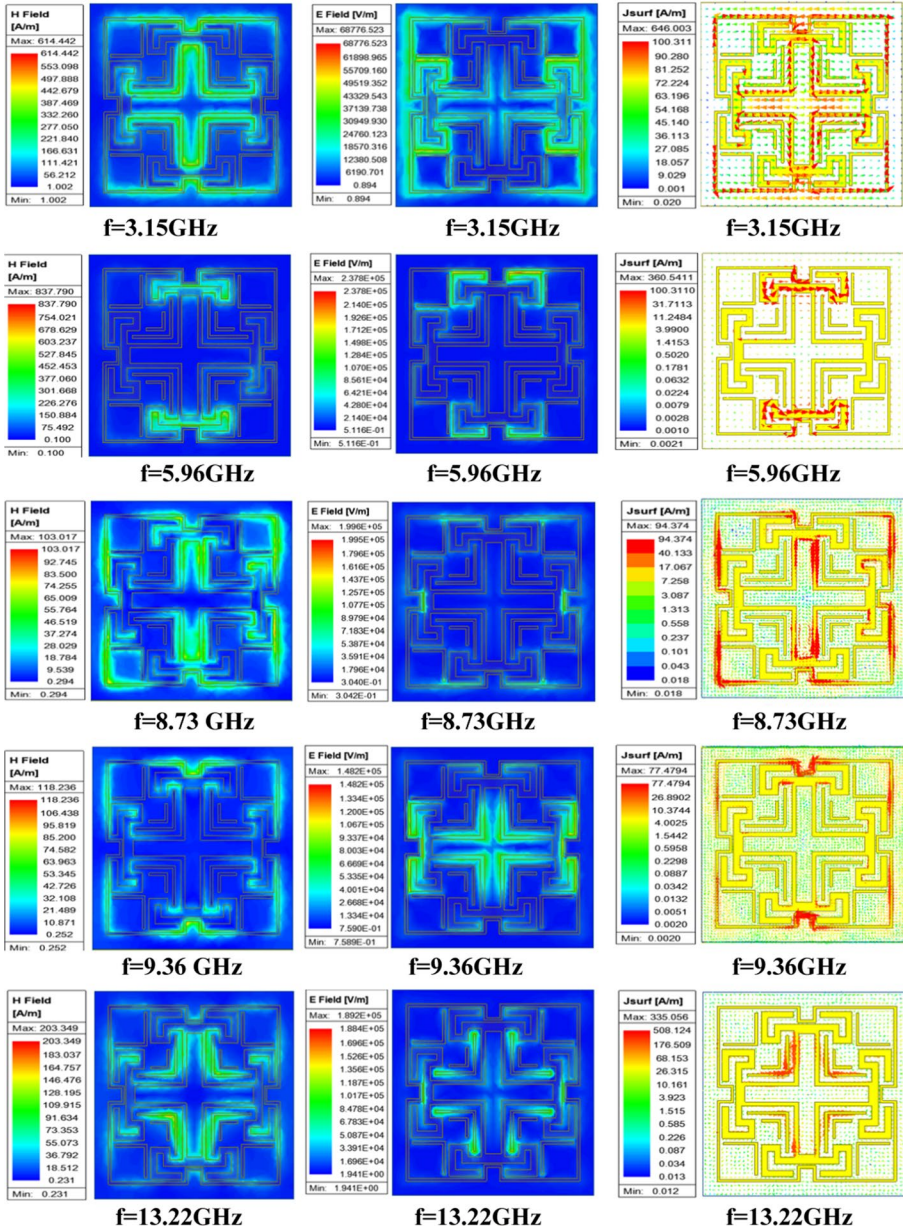


Fig. 10 Magnetic (H) field, electric (E) field, and surface current distribution presentations for the unit cell MMA

$L_8=0.5$ nH, $C_1=0.025578$ pF, $C_2=0.798$ pF, $C_3=0.1001$ pF, $C_4=1.11$ pF, $C_5=0.02607$ pF, $C_6=0.318$ pF, $C_7=0.0192355$ pF, $C_8=0.03683$ pF, $C_9=0.03856$ pF, $C_{10}=0.137$ pF, $C_{11}=0.010614$ pF, $C_{12}=0.21181343$ pF, $C_{13}=0.014351$ pF,

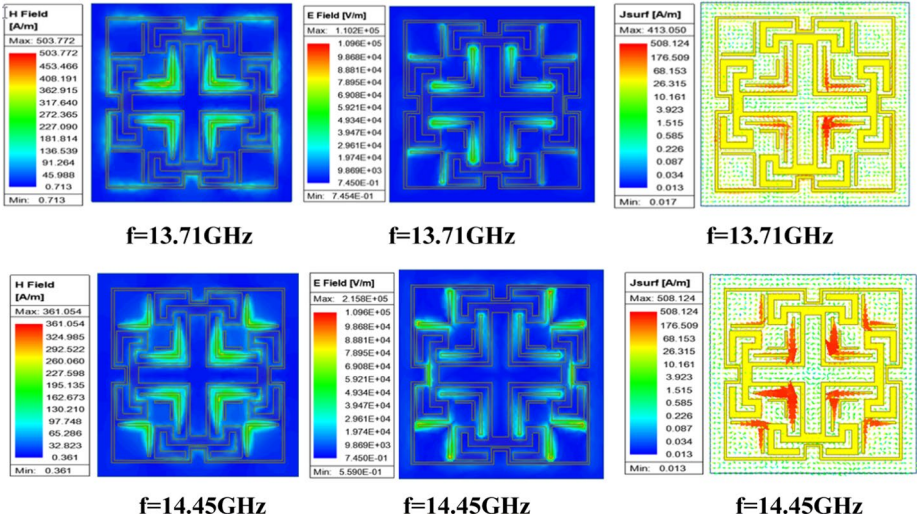


Fig. 10 (continued)

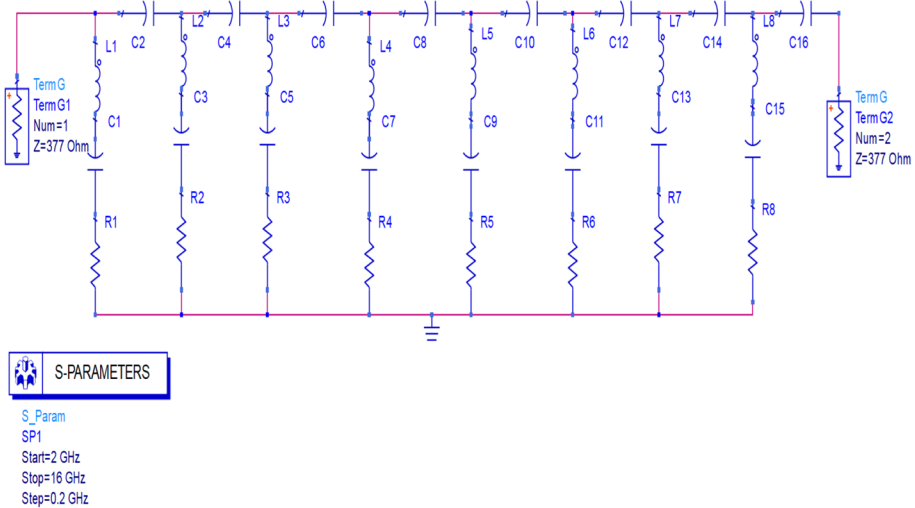
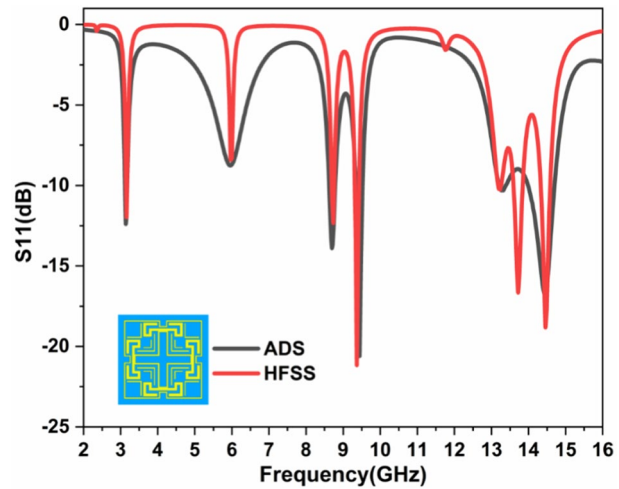


Fig. 11 ECM of the proposed hepta-band MMA

$C_{14}=0.564$ pF, $C_{15}=0.01175$ pF, $C_{16}=0.3$ pF, $R_1=58 \Omega$, $R_2=36 \Omega$, $R_3=29.5 \Omega$, $R_4=36 \Omega$, $R_5=9.54 \Omega$, $R_6=25.995 \Omega$, $R_7=22.8 \Omega$, $R_8=25 \Omega$. The impedance for the two surfaces (patch and ground) equals the impedance of the free space (377Ω). Figure 12 shows the S11 values obtained by both ADS and HFSS software. It is remarkable that for first four resonance frequencies, the values of the S11 obtained from HFSS and ADS are matched perfectly. For the Ku band, slight variations in S11 values are noted

Fig. 12 S11 simulation results using HFSS and ADS



as obtained by ADS software, which may be due to the presence of the broad absorption band that characterizes the Ku band.

5 Parametric structural analysis and performance comparison

The geometry of the metallic components that frames the patch of the MMA structure affects the effective inductance and capacitance. When the length and width of a metal element in the patch vary, this leads to variations in its effective inductance. Similarly, changes in the gap between the metal elements of the patch influence its effective capacitance. These changes in the dimensions of the structural parameters affect both the effective inductance and capacitance, which can have an impact on the coupling between the patch elements and lead to changes in the absorption profile. In this section, the effects of variations in the geometrical parameters of this proposed MMA are

Fig. 13 The impact of parameter 'a' on the absorption profile

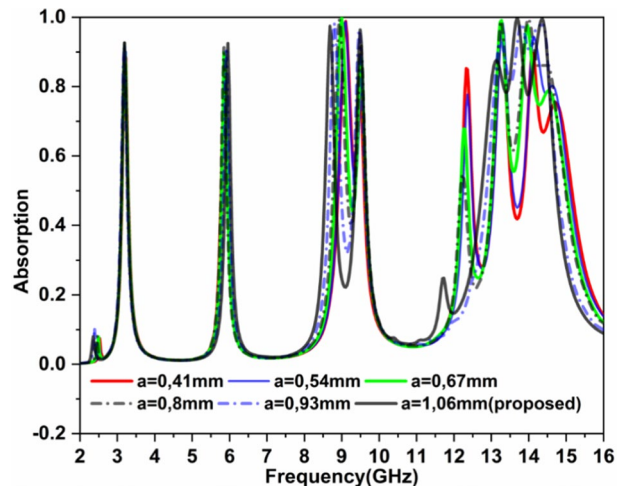


Fig. 14 The impact of parameter 'w' on the absorption profile

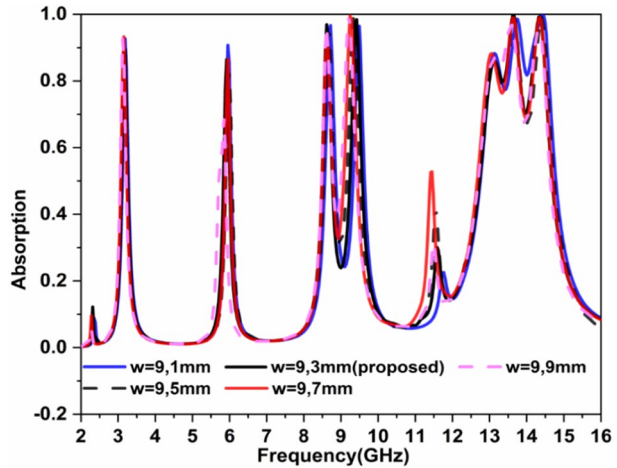
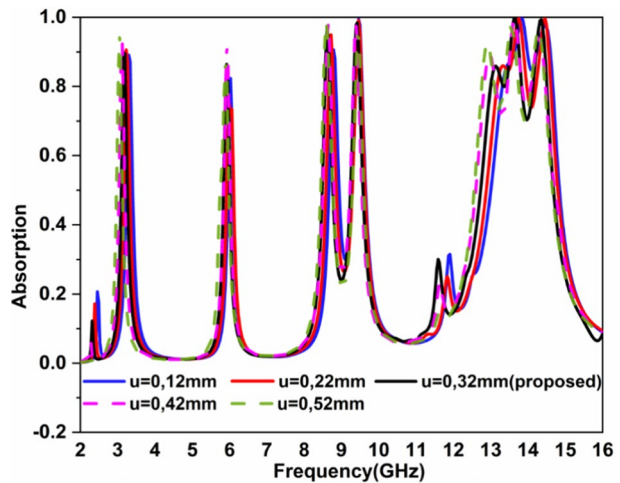


Fig. 15 The impact of parameter 'u' on the absorption profile



investigated and discussed. Several parameters for this MMA can be varied to obtain a strong resonance. The length 'a' of the square part of the Resonator-A has been varied from 0.41 to 1.06 mm, with all other parameters held constant. The impact of parameter 'a' on the absorption profile is illustrated in Fig. 13. When the parameter 'a' increases in its value, the magnitude of fourth absorption band increases but the third peak decreases and shifts slightly toward the low frequencies, while the magnitudes of first two bands remains unchanged. For the Ku band, the first absorption peak decreases, and the peak magnitudes of last two bands are increased. The parameter 'w' varies from 9.1 to 9.9 mm, and its influence on the absorption spectrum is plotted in Fig. 14. As 'w' increases, the first and third bands are not affected, while the second bands lightly alternate between increased and decreased values. The fourth band increases and shifts slightly towards lower frequencies, as do the peak absorption of the Ku band, which also exhibit a slight shift towards lower frequencies. Furthermore, Fig. 15 shows the effect of the variation in Resonator-B's parameter 'u' from 0.12 to 0.52 mm on the absorption

Table 4 Comparative study of the proposed multi band metamaterial (MTM) absorber with other reported absorber designs

References	Unit cell size	Operating frequency	Resonant frequency (GHz)	Absorption (%)	FWHM bandwidth (GHz)
Kalraiya et al. (2021)	$0.23\lambda_0 \times 0.23\lambda_0 \times 0.0065\lambda_0$	C, X	6.1, 9.2, 11.6	95, 96, 97	0.16, 0.24, 0.26
Chaitanya et al. (2020)	$0.305\lambda_0 \times 0.305\lambda_0 \times 0.0135\lambda_0$	C, X	5.09, 6.53, 7.95, 10.12, 11.57	98.80, 97.97, 97.38, 97.62, 98.57	0.25, 0.20, 0.27, 0.43, 0.41
Garg and Jain. (2020)	$0.11\lambda_0 \times 0.11\lambda_0 \times 0.011\lambda_0$	S, C, X, Ku	3.35, 5.1, 9.5, 11.1, 16.9	99.59, 95.49, 97.5, 99.25, 93.89	0.11, 0.21, 0.31, 0.34, 0.44
Singh and Gupta (2021)	$0.11\lambda_0 \times 0.11\lambda_0 \times 0.01\lambda_0$	S, X, Ku	3.2, 5.32, 11.15, 19.73	95.75, 95.93, 97.69, 95.64	0.09, 0.22, 0.41, 0.7
Islam et al. (2021)	$0.101\lambda_0 \times 0.101\lambda_0 \times 0.019\lambda_0$	S, C, X, Ku	3.80, 5.65, 8.45, 10.82, 15.92	97.87, 93.65, 92.66, 99.95, 99.86	0.13, 0.24, 0.51, 0.54, 1.34
Singh and Gupta (2022)	$0.135\lambda_0 \times 0.135\lambda_0 \times 0.0104\lambda_0$	C, X, Ku	5.20, 9.99, 14.56	99.81, 99.77, 99.68	0.18, 0.32, 0.56
Jahan et al. (2023)	$0.129\lambda_0 \times 0.129\lambda_0 \times 0.0255\lambda_0$	C, X, Ku	4.87, 7.49, 11.78, 13.09	99.9, 99.9, 99.9, 99.8	0.2, 0.8, 0.5, 0.3
Ishrat Jahan et al. (2023)	$0.130\lambda_0 \times 0.130\lambda_0 \times 0.0229\lambda_0$	C, X, Ku	4.37, 7.08, 9.38, 10.65	99.8, 99.9, 99.9, 99.9	0.2, 1, 0.7, 0.7
Binda et al. (2023)	$0.167\lambda_0 \times 0.167\lambda_0 \times 0.0134\lambda_0$	S, X, Ku	5.026, 8.852, 11.37, 15.036	95.67, 99.16, 95.97, 97.02	0.18, 0.36, 0.42, 0.58
This work	$0.168\lambda_0 \times 0.168\lambda_0 \times 0.0168\lambda_0$	S, C, X, Ku	3.15, 5.96, 8.73, 9.36, 13.22, 13.71, 14.45	93.65, 85.75, 94.14, 99.51, 90.55, 97.87, 98.68	0.20, 0.19, 0.30, 0.34, 2.04

profile. With an increase in 'u', all of the absorption bands shift towards the lower frequencies, so the first and third absorption peaks increase, while the second band fluctuates between a minimum to maximum absorption values.

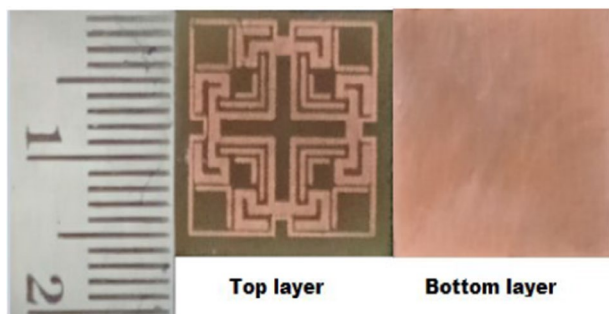
Table 4 compares the multiband MMA presented in this paper with some other recent MMAs reported in the literature. The performance analysis has been executed and presented in terms of the electrical dimension of the unit cell, the frequency band, the number of resonances with their absorption percentages, and the bandwidth FWHM. The suggested MMA achieves septuple absorption peaks within the microwave S, C, X, and Ku bands and has the largest absorption bandwidth FWHM as compared to other absorber designs as projected in comparison table. Furthermore, when compared to previously published research articles, this absorber is competitive in terms of its dimension.

6 Experimental validation

To validate the simulation results, the prototype of absorber's unit cell is fabricated on an FR4-Epoxy substrate (tangent loss of 0.02, dielectric constant of $\epsilon_r = 4.4$). Figure 16 shows the prototype from two different perspectives, top and bottom views with a ruler showing its measurements.

The reflection coefficient of the prototyped MMA is measured using vector network analyzer (VNA) and on the basis of these measurement results the absorption coefficient ($A(f) = 1 - |S_{11}|^2$) and the absorption coefficient is displayed in Fig. 17. The manufactured prototype of the suggested absorber exhibits seven absorption peaks at 3.14, 6.06, 8.69, 9.38, 13.15, 13.68, and 14.49 GHz with an absorption level of 90.47, 85.11, 92.78, 98.99, 92.24, 97.30, and 98.79%, respectively. For the four application bands, the corresponding measured FWHM bandwidths are 0.21 GHz (3.36–2.98 GHz) for the S-band, 0.19 GHz (6.13–5.94 GHz) for the C-band, 0.35 GHz (9.01–8.66 GHz) and 0.44 GHz (9.64–9.20 GHz) for the X-band, and 2.14 GHz (14.92–12.78) for the Ku-band. The measurement results are compatible with those of the simulation. However, the presence of slight differences between measurement and simulation results are obvious, due to the small size of the manufactured prototype and alignment imperfections, fabrication and measurement tolerances.

Fig. 16 Top and bottom faces of the manufactured unit cell



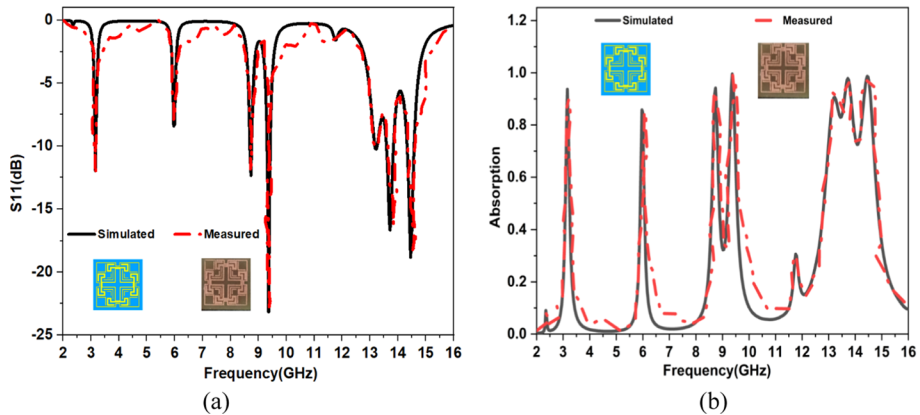


Fig. 17 Comparison of measurement and simulation results **a** S11 parameters, **b** absorption coefficient

7 Conclusion

A novel polarization-insensitive multi-band metamaterial (MTM) absorber is presented in this proposed article. The unit cell of the optimally designed metamaterial based absorber consists of three resonators, which are designed on a low cost FR-4 substrate with an overall size of 13.8 mm × 13.8 mm. The absorption mechanism is examined by analyzing the distribution of electric and magnetic fields, as well as surface currents. The extraction of the permeability and permittivity parameters indicates that this structure exhibits a single negative (SNG) response. The design and simulation studies were performed using a high frequency structure simulator (HFSS). The equivalent circuit model (ECM) based analysis for the unit cell of the proposed absorber was also investigated. The results analyzed through the simulation tool (HFSS) and equivalent circuit model (ECM) shows good agreement. To confirm the reliability of simulation results, the prototype model was fabricated and experimentally tested. The measurement results validate the specific design approach of this proposed metamaterial absorber (MMA). The suggested absorber exhibits seven absorption peaks at 3.14, 6.06, 8.69, 9.38, 13.15, 13.68, and 14.49 GHz with absorption rates of 90.47, 85.11, 92.78, 98.99, 92.24, 97.30, and 98.79%. The proposed MMA finds widespread uses in sensing, radar, and satellite communications in microwave frequency regions.

Author contributions All authors contributed to the study, conception, design and simulations. Data collection, analysis, and simulation were performed by KE, NJ, and SD. Additional input to analysis, model improvement, and simulation was given by TI, BTPM, TEL-A. All authors contributed to complete the writing and presentation of the whole manuscript. All the authors have read and approved the final manuscript.

Funding No funding is available for this work presented in this manuscript.

Data availability All the data generated during and/or analyzed during the current study are available from the corresponding author on reasonable request.

Code availability Implemented through High Frequency Structure Simulator (HFSS) software.

Declarations

Conflict of interest The authors declare that they have no conflict of interest or competing interests.

Consent for publication The authors confirm that there is informed consent to the publication of the data contained in the article.

Consent to participate Informed consent was obtained from all authors.

Ethics approval This research study complied with the ethical standards.

References

- Abdulkarim, Y.I., Altintas, O., Karim, A.S., Awl, H.N., Muhammadsharif, F.F., Alkurt, F.Ö., Bakir, M., Appasani, B., Karaaslan, M., Dong, J.: Highly sensitive dual-band terahertz metamaterial absorber for biomedical applications simulation and experiment. *ACS Omega* **7**, 38094–38104 (2022). <https://doi.org/10.1021/acsomega.2c06118>
- Abouelez, A.E., Abdalaleem, M.N.: Design and analysis of quad-band polarization-insensitive infrared perfect metamaterial absorber with a wide-incident angle. *Opt. Quantum Electron.* **55**, 1045 (2023). <https://doi.org/10.1007/s11082-023-05298-3>
- Ali, H.O., Al-Hindawi, A.M., Abdulkarim, Y.I., Karaaslan, M.: New compact six-band metamaterial absorber based on Closed Circular Ring Resonator (CCRR) for Radar applications. *Opt. Commun.* **503**, 127457 (2022a). <https://doi.org/10.1016/j.optcom.2021.127457>
- Ali, H.O., Al-Hindawi, A.M., Abdulkarim, Y.I., Nugoolcharoenlap, E., Tippo, T., Alkurt, F.Ö., Altinta, O., Karaaslan, M.: Simulated and experimental studies of a multi-band symmetric metamaterial absorber with polarization independence for radar applications. *Chin. Phys. B* **31**, 058401 (2022b). <https://doi.org/10.1088/1674-1056/ac2b1c>
- Balanis, C.A.: *Advanced Engineering Electromagnetics*. Wiley (2012)
- Binda, P., Singh, R.K., Mitharwal, R.: An ultra-thin, polarization free wide-angle stable quad-band metamaterial absorber for applications in C, X, and Ku bands. *AEU Int. J. Electron. Commun.* **171**, 154925 (2023). <https://doi.org/10.1016/j.aeue.2023.154925>
- Chaitanya, G., Neema, J., Dubey, A.: Penta-band polarization controlled ultrathin metamaterial absorber for microwave applications. In: 2020 IEEE International Conference on Electronics, Computing and Communication Technologies (CONECCT), pp. 1–6, Bangalore, India (2020). <https://doi.org/10.1109/CONECCT50063.2020.9198390>.
- Chaurasiya, D., Ghosh, S., Bhattacharyya, S., Bhattacharya, A., Srivastava, K.V.: Compact multi-band polarisation-insensitive metamaterial absorber. *IET Microw. Antennas Propag.* **10**, 94–101 (2016). <https://doi.org/10.1049/iet-map.2015.0220>
- Dewangan, L., Mishra, N.K.: Multiband polarization insensitive metamaterial absorber for radar cross-section reduction. *AEU Int. J. Electron. Commun.* **168**, 154706 (2023). <https://doi.org/10.1016/j.aeue.2023.154706>
- EL-Wasif, Z., Ismail, T., Hamdy, O.: Design and optimization of highly sensitive multi-band terahertz metamaterial biosensor for coronaviruses detection. *Opt. Quantum Electron.* **55**, 604 (2023). <https://doi.org/10.1007/s11082-023-04906-6>
- Garg, P., Jain, P.: Novel ultrathin penta-band metamaterial absorber. *AEU Int. J. Electron. Commun.* **116**, 153063 (2020). <https://doi.org/10.1016/j.aeue.2020.153063>
- Gau, J.-R., Burnside, W., Gilreath, M.: Chebyshev multilevel absorber design concept. *IEEE Trans. Antennas Propag.* **45**, 1286–1293 (1997). <https://doi.org/10.1109/8.611249>
- Hakim, M.L., Alam, T., Soliman, M.S., Sahar, N.M., Baharuddin, M.H., Almalki, S.H.A., Islam, M.T.: Polarization insensitive symmetrical structured double negative (DNG) metamaterial absorber for Ku-band sensing applications. *Sci. Rep.* **12**, 479 (2022). <https://doi.org/10.1038/s41598-021-04236-1>
- Hakim, M.L., Alam, T., Islam, M.T., Alsaif, H., Soliman, M.S.: Polarization-independent fractal square splits ring resonator (FSSRR) multiband metamaterial absorber/artificial magnetic conductor/sensor for Ku/K/Ka/5G (mm-wave) band applications. *Measurement* **210**, 112545 (2023). <https://doi.org/10.1016/j.measurement.2023.112545>

- Hannan, S., Islam, M.T., Sahar, N.M., Mat, K., Chowdhury, M.E.H., Rmili, H.: Modified-segmented splitting based polarization and angle-insensitive multi-band metamaterial absorber for X, Ku and K band applications. *IEEE Access* **8**, 144051–144063 (2020). <https://doi.org/10.1109/ACCESS.2020.3013011>
- Hannan, S., Islam, M.T., Faruque, M.R.I., Rmili, H.: Polarization-independent perfect metamaterial absorber for C, X and Ku band applications. *J. Mater. Res. Technol.* **15**, 3722–3732 (2021). <https://doi.org/10.1016/j.jmrt.2021.10.007>
- Hannan, S., Islam, M.T., Almalki, S.H.A., Faruque, M.R.I., Islam, M.S.: Rotational symmetry engineered, polarization and incident angle-insensitive, perfect metamaterial absorber for X and Ku band wireless applications. *Sci. Rep.* **12**, 3740 (2022a). <https://doi.org/10.1038/s41598-022-07824-x>
- Hannan, S., Islam, M.T., Soliman, M.S., Faruque, M.R.I., Misran, N., Islam, M.S.: A co-polarization insensitive metamaterial absorber for 5G n78 mobile devices at 3.5 GHz to reduce the specific absorption rate. *Sci. Rep.* **12**, 11193 (2022b). <https://doi.org/10.1038/s41598-022-15221-7>
- Hannan, S., Islam, M.T., Soliman, M.S., Mohd Sahar, N.B., Jit Singh, M.S., Faruque, M.R.I., Alzamil, A.: A filling-factor engineered, perfect metamaterial absorber for multiple applications at frequencies set by IEEE in C and X bands. *J. Mater. Res. Technol.* **19**, 934–946 (2022c). <https://doi.org/10.1016/j.jmrt.2022.05.071>
- Hossain, M.B., Faruque, M.R.I., Islam, M.T., Singh, M., Jusoh, M.: Triple band microwave metamaterial absorber based on double E-shaped symmetric split ring resonators for EMI shielding and stealth applications. *J. Mater. Res. Technol.* **18**, 1653–1668 (2022). <https://doi.org/10.1016/j.jmrt.2022.03.079>
- Hossain, M.B., Faruque, M.R.I., Islam, M.T.: Double elliptical resonator based quadruple band metamaterial absorber for EMI shielding applications in microwave regime. *Alex. Eng. J.* **69**, 193–206 (2023). <https://doi.org/10.1016/j.aej.2023.01.035>
- Hrubar, S.: Waveguide experiments to characterize properties of SNG and DNG metamaterials. In: Eng-beta, N., Ziolkowski, R.W. (eds.) *Metamaterials*, pp. 87–111. Wiley, Hoboken (2006). <https://doi.org/10.1002/0471784192.ch3>
- Ishrat Jahan, M., Rashed Iqbal Faruque, M., Bellal Hossain, M.: An X-shaped triple split ring resonator-based metamaterial perfect absorber with quad-band incident and polarization angle insensitivity for C, X, and Ku band applications. *J. Magn. Magn. Mater.* **580**, 170940 (2023). <https://doi.org/10.1016/j.jmmm.2023.170940>
- Islam, M.R., Islam, M.T., Moniruzzaman, M., Samsuzzaman, M., Arshad, H.: Penta band single negative meta-atom absorber designed on square enclosed star-shaped modified split ring resonator for S-, C-, X- and Ku-bands microwave applications. *Sci. Rep.* **11**, 8784 (2021). <https://doi.org/10.1038/s41598-021-87958-6>
- Jahan, M.I., Faruque, M.R.I., Hossain, M.B., Khandaker, M.U., Elsayed, F., Salman, M., Osman, H.: Quad-band metamaterial perfect absorber with high shielding effectiveness using double X-shaped ring resonator. *Materials* **16**, 4405 (2023). <https://doi.org/10.3390/ma16124405>
- Kalraiya, S., Chaudhary, R.K., Gangwar, R.K.: Polarization independent triple band ultrathin conformal metamaterial absorber for C- and X-frequency bands. *AEU Int. J. Electron. Commun.* **135**, 153752 (2021). <https://doi.org/10.1016/j.aeue.2021.153752>
- Kong, X., Zhang, H., Dao, R., Liu, G.: Comment on “design of a quad-band wide-angle microwave meta-material absorber.” *J. Electron. Mater.* **48**, 4166–4169 (2019). <https://doi.org/10.1007/s11664-019-07194-7>
- Landy, N.I., Bingham, C.M., Tyler, T., Jokerst, N., Smith, D.R.: Design, theory, and measurement of a polarization-insensitive absorber for terahertz imaging. *Phys. Rev. B* **79**, 125104 (2009). <https://doi.org/10.1103/PhysRevB.79.125104>
- Luukkonen, O., Maslovski, S.I., Tretyakov, S.A.: A stepwise Nicolson–Ross–Weir-based material parameter extraction method. *IEEE Antennas Wirel. Propag. Lett.* **10**, 1295–1298 (2011). <https://doi.org/10.1109/LAWP.2011.2175897>
- Lv, Y., Liu, W., Tian, J., Yang, R.: Broadband terahertz metamaterial absorber and modulator based on hybrid graphene-gold pattern. *Phys. E Low Dimens. Syst. Nanostruct.* **140**, 115142 (2022). <https://doi.org/10.1016/j.physe.2022.115142>
- Mahmud, S., Islam, S.S., Almutairi, A.F., Islam, M.T.: A wide incident angle, ultrathin, polarization insensitive metamaterial absorber for optical wavelength applications. *IEEE Access* **8**, 129525–129541 (2020)
- Michielssen, E., Sajer, J.-M., Ranjithan, S., Mittra, R.: Design of lightweight, broad-band microwave absorbers using genetic algorithms. *IEEE Trans. Microw. Theory Tech.* **41**, 1024–1031 (1993). <https://doi.org/10.1109/22.238519>
- Moniruzzaman, M., Islam, M.T., Muhammad, G., Singh, M.S.J., Samsuzzaman, M.: Quad band metamaterial absorber based on asymmetric circular split ring resonator for multiband microwave applications. *Results Phys.* **19**, 103467 (2020). <https://doi.org/10.1016/j.rinp.2020.103467>

- Munaga, P., Ghosh, S., Bhattacharyya, S., Chaurasiya, D., Srivastava, K.V.: An ultra-thin dual-band polarization-independent metamaterial absorber for EMI/EMC applications. In: 2015 9th European Conference on Antennas and Propagation (EuCAP). IEEE, pp. 1–4
- Paul, C.R.: Inductance: Loop and Partial. Wiley (2009)
- Ren, Z., Lin, Z., Zhi, X., Li, M.: Double-layer broadband perfect metamaterial absorber and its potential for refractive index sensing. *Opt. Mater.* **99**, 109575 (2020). <https://doi.org/10.1016/j.optmat.2019.109575>
- Saadeldin, A.S., Sayed, A.M., Amr, A.M., Sayed, M.O., Hameed, M.F.O., Obayya, S.S.A.: Broadband polarization insensitive metamaterial absorber. *Opt. Quantum Electron.* **55**, 652 (2023). <https://doi.org/10.1007/s11082-023-04881-y>
- Shuvo, M.M.K., Hossain, M.I., Mahmud, S., Rahman, S., Topu, M.T.H., Hoque, A., Islam, S.S., Soliman, M.S., Almalki, S.H.A., Islam, M.S., Islam, M.T.: Polarization and angular insensitive bendable metamaterial absorber for UV to NIR range. *Sci. Rep.* **12**, 4857 (2022). <https://doi.org/10.1038/s41598-022-08829-2>
- Singh, R.K., Gupta, A.: A wrenched-square shaped polarization independent and wide angle stable ultra-thin metamaterial absorber for S-band, X-band and Ku-band applications. *AEU Int. J. Electron. Commun.* **132**, 153648 (2021). <https://doi.org/10.1016/j.aeue.2021.153648>
- Singh, R.K., Gupta, A.: Theoretical and experimental study of angle independent conformal tri-band metamaterial absorber design for industrial and defense applications. *Int. J. RF Microw. Comput. Aided Eng.* **32**, e23402 (2022). <https://doi.org/10.1002/mmce.23402>
- Wartak, M.S., Tsakmakidis, K.L., Hess, O.: Introduction to metamaterials. *Phys. Canada* **67**(1), 30–34 (2011)
- Woodley, J., Mojahedi, M.: On the signs of the imaginary parts of the effective permittivity and permeability in metamaterials. *J. Opt. Soc. Am. B* **27**, 1016 (2010). <https://doi.org/10.1364/JOSAB.27.001016>
- Wu, J., Sun, Y., Wu, B., Sun, C., Wu, X.: Perfect metamaterial absorber for solar energy utilization. *Int. J. Therm. Sci.* **179**, 107638 (2022). <https://doi.org/10.1016/j.ijthermalsci.2022.107638>
- Zadeh, A., Karlsson, A.: Capacitive circuit method for fast and efficient design of wideband radar absorbers. *IEEE Trans. Antennas Propag.* **57**, 2307–2314 (2009). <https://doi.org/10.1109/TAP.2009.2024490>
- Zhang, Y., Dong, H., Mou, N., Chen, L., Li, R., Lv, Y., Zhang, L.: High-performance broadband electromagnetic interference shielding optical window based on a metamaterial absorber. *Opt. Express* **28**, 26836–26849 (2020). <https://doi.org/10.1364/OE.401766>
- Ziolkowski, R.: Design, fabrication, and testing of double negative metamaterials. *IEEE Trans. Antennas Propag.* **51**, 1516–1529 (2003). <https://doi.org/10.1109/TAP.2003.813622>

Publisher's Note Springer Nature remains neutral with regard to jurisdictional claims in published maps and institutional affiliations.

Springer Nature or its licensor (e.g. a society or other partner) holds exclusive rights to this article under a publishing agreement with the author(s) or other rightsholder(s); author self-archiving of the accepted manuscript version of this article is solely governed by the terms of such publishing agreement and applicable law.

Authors and Affiliations

Karim Errajaji¹ · Nawfal Jebbor¹ · Sudipta Das² · Tanvir Islam³ ·
Boddapati Taraka Phani Madhav⁴ · Tarik El-Arrouch⁵

✉ Sudipta Das
sudipta.das1985@gmail.com

¹ Electronics Instrumentation and Intelligent Systems Team, ER2TI Laboratory, Department of Physics, Faculty of Sciences and Technics, Moulay Ismail University of Meknes, Errachidia, Morocco

² Department of Electronics and Communication Engineering, IMPS College of Engineering and Technology, Malda, West Bengal, India

³ Department of Electrical and Computer Engineering, University of Houston, Houston, TX, USA

⁴ Antennas and Liquid Crystals Research Centre, Department of ECE, Koneru Lakshmaiah

Education Foundation, Vijayawada, Andhra Pradesh, India

⁵ Faculty of Sciences and Technics, Signals, Systems and Components Laboratory (LSSC), Sidi Mohamed Ben Abdellah University, Fez, Morocco